

ABSTRACT

Title of thesis: IN-SITU CONFORMAL 3D PRINTING FOR TARGETED REPAIRS

Team PRINT: Rohith Chintala, Brendan Cutick, Tyler Han, Elizabeth Myers, Eric Oh, Aidan Sandman-Long, Cynthia Sheng, Nathan Spicer-Davis

Thesis directed by: Dr. Steven Mitchell
Department of Mechanical Engineering

David Edelen
Additive Manufacturing Lead KAIROS, Inc

Additive manufacturing is an emerging technology whose users seek to benefit from repair methods to reduce time and material costs. We explore an application of the technology to targeted repairs, such as mending holes or cracks, on 3D printed parts by using conformal tool-pathing, combining the precision of additive manufacturing with the strength and homogeneity of material adhesion. To characterize the efficacy of targeted 3D printing repair for FFF plastics, repair configurations varying in shape, size, material, infill and loading type are tested in 3-point bending for structural strength and strain. We provide and summarize the collected data in addition to a structural analysis and optimization of parameters relevant to reparative 3D printing.

Team PRINT Thesis

by

Rohith Chintala, Brendan Cutick, Tyler Han, Elizabeth Myers, Eric Oh, Aidan

Sandman-Long, Cynthia Sheng, Nathan Spicer-Davis

Table of Contents

Chapter 1: Introduction

Chapter 2: Literature Review

2.1 Overview

2.2 Materials

 2.2.1 PLA

 2.2.2 ABS

 2.2.3 Comparison

2.3 Structural Analysis

 2.3.1 TBD

2.4 Slicing and Gcode

 2.4.1 Printing on Concave Surfaces

2.5 Existing Work regarding Infill Patterns

 2.5.1 Optimal Print Settings

 2.5.1 Cost Analysis

Chapter 3: Experimentation

3.1 Introduction/Motivation

3.2 Hypothesis(es)

3.3 Testing Standards

 3.3.1 ASTM D638

 3.3.2 ASTM D790

3.4 Materials & Equipment

 3.4.1 Printing

3.4.2 Press

3.5 Experiment/Steps Taken

3.5.1 Infill Testing

3.5.2 Damage Testing

Chapter 4: Results

4.1 Introduction

4.2 Data/Plots

4.3 Structural Analysis

4.4 Discussion/Conclusion

Chapter 5: Future Work

5.1 Adaptive In-Situ Printing

5.2 Materials

5.3 Extreme Environment

Appendix

I. Timeline

II. Budget

III. Mentor Feedback

IV. Glossary

References



Chapter 1: Introduction

In order to produce a component for any project, there are currently two methods of production: additive and subtractive manufacturing. Additive Manufacturing (AM) is the process of depositing material in predefined locations to create a structure. 3D printing is a popular example of AM. There seems to be few limits to the possibilities of additive manufacturing in mechanical design and manufacturing. In addition to producing scale models and rapid prototyping, AM is capable of making complex, functional, and durable structures. For example, rocket nozzles capable of withstanding the high pressures and thermal stresses of rocket propulsion [1]. Industries are taking seriously the engineering applications of 3D printed structures in their products: a 3D printed airplane structure was subjected to representative loads applied to the fuselage and wings [2]. Both of these developments demonstrate that AM can be used in high-stress applications and that there is a trend in trying to replace current manufacturing techniques with lower cost, light-weight AM materials and processes. Given that 3D printed structures are likely to become increasingly common and used for crucial components in a variety of complex systems, we believe it is necessary to investigate how the operational lifetimes of such components can be extended and material waste can be minimized so that this relatively new technology can be used as responsibly as possible.

In mechanical structures, frequently used components will gradually wear over time. A component such as the interface for a motor shaft is critical to the operation of the greater mechanism but even superficial damages can render it useless (e.g. stripped locking grooves). Once the damage is severe enough, a typical solution is to replace the component entirely. Depending on the size of the component and the severity of the damage, this can be very

wasteful in terms of the materials and time needed to reprint and replace the damaged component.

Some applications may not even have the option of replacing damaged components, such as in the aerospace industry. Damage to rover wheels has been cited as a reason for being unable to complete mission objectives and limiting the areas that are accessible to the rover [3]. With no replacement parts, no accessible servicing stations, and no way to return the rover to Earth, the system simply must be able to endure whatever damage it may experience. Similarly, the design lifetime of a satellite takes into account the rate of damage it is expected to experience from micro-meteoroids and other orbital debris.

It would be far more advantageous if a repair was applied directly to the damaged parts, preserving structural integrity and shape to enable continued use. While one can approach direct repair using either subtractive or additive methods, several industries such as those in aeronautics or astronautics have directed attention towards additive manufacturing, taking advantage of AM's quick and cheap prototyping. Thus, it would be desirable to have an additive repair method which aligned with the interests of these industries. Having the ability to repair damaged components using AM could drastically increase a system's lifetime, and even allow for an entirely more efficient design.

In our review of the existing literature, we found that AM for in-situ repairs has not yet been thoroughly investigated. This poses several potential questions and criticisms which should be answered before proceeding with such technology: Can a repair effectively reinstate a component's viability of operation? Is the repair worth the time and material costs? Under what circumstances can a component be repaired? Clearly, the answers to these questions will vary by application. In the following work, we choose to investigate Fused Filament Fabrication (FFF)

parts. FFF parts are widespread in both hobbyist and engineering industries. Plastics like Polylactic Acid (PLA) are commonly used in prototypes and engineering drafts. In addition, considering the resources available to us, proceeding with FFF and plastics (as opposed to metal fabrication methods like Selective Laser Sintering) present the most feasible option while permitting proof-of-concept experiments.

In an attempt to quantify a repair's structural integrity, the experiments (discussed further in Chapter 3) include three-point bending of repaired structures while varying properties of print such as infill percentage, infill pattern, and plastic material. By thoroughly collecting and analyzing data, we will be able to give unambiguous answers to the above questions and identify new questions that we believe would be worth investigating in the future. We are particularly interested in optimization of targeted 3D printed repairs, and our work suggests that there exist parameters which improve structural strength and efficiency which are not immediately intuitive.

The following chapter will delve deeply into the background of the problem and provide context for our proposed solution. After that, a discussion of the methodology used will provide full detail of our experimentation, data collection, and data analysis methods as well as the motivation behind them. Following the methodology, we will present and discuss our results, and in doing so, we will answer the questions we have identified as being relevant to determining whether our proposed repair method is "effective." Finally, we will end with a discussion of what future research we recommend be done in order to build off of our work and progress further towards an implementable solution.

[1] N. Quigley and J. E. Lyne, “Development of a Three-Dimensional Printed, Liquid-Cooled Nozzle for a Hybrid Rocket Motor,” *Journal of Propulsion and Power*, vol. 30, no. 6, pp. 1726–1727, 2014, doi: [10.2514/1.B35455](https://doi.org/10.2514/1.B35455).

[2] R. M. Taylor *et al.*, “Design Optimization, Fabrication, and Testing of a 3D Printed Aircraft Structure Using Fused Deposition Modeling,” in *AIAA Scitech 2020 Forum*, American Institute of Aeronautics and Astronautics. doi: [10.2514/6.2020-1924](https://doi.org/10.2514/6.2020-1924).

[3] Same one from lit revie-Finish 423 HW6



Chapter 2: Literature Review

2.1 Introduction and Applications

The following literature review presents a survey of recent or related research that may aid the development of an in situ 3D printer in the areas that appear to require the most attention.

The full implementation of such a device is needed in order to make repairs to structures that are in unsafe or inaccessible environments for humans. Repairs for on-orbit satellites and extraterrestrial rovers are applications where the technology may be invaluable. Historically, rovers have experienced physical damage that has compromised abilities to fully complete missions [1]. This includes wheel damage that has led to the mission sites being restricted to relatively flat terrain that is not rocky [1]. In figure 1, the wheel thickness is 0.75mm and the approximate diameter of the hole is 3cm. For this future application, voids on the scales of 1cm -

5cm would be ideal for the applications of repairing these holes. It would be possible for a 3D printer to attach to a robotic arm and navigate to a desired location for printing. Implementation of a robotic arm capable of these wheel repairs aligns with NASA's efforts [2] toward the potential of sending multiple small and collaborative rovers on missions. In this situation, it is plausible for there to be a robot specifically designed to repair other rovers in situ to aid in lengthening future missions and mitigating unforeseen damage.



Figure 1. Image from MastCam of Mars Curiosity Wheel Damage. [3]

Applications can also be found in the aviation industry. [4] describes how an in situ 3D printer can be used to repair components more easily than welding, which is the current method. 3D printing has a lower operating temperature than welding, eradicating the struggle of thermal damage to components normally caused by welding. [4]. This allows parts to be repaired to near net-shape condition with less wasted material and a stronger finish [4]. The process is also especially useful in the aviation industry because parts must have specific contours that can be more easily matched by conformal printing to decrease drag [4].

A specific example of this was recently tested by Saab AB, a Swedish aerospace company, in March 2021. The company tested how additive manufacturing could be applied to a

damaged component of their aircraft in a simulated battlefield setting. They achieved this by removing a panel from their aircraft, scanning the void, and 3D printing an exact replica of the missing piece using a nylon PA2200 polymer [5]. Since there was no 3D model of the aircraft piece, it had to be scanned. In real life, damage to aircrafts will be unpredictable, so it is important that they have a way to do this. Applications for this type of repair include rapid repairs for jet aircraft that may have sustained damage during missions in remote locations. A 3D printed piece could save time on turnaround.



Figure 2. Saab JAS 39 Gripen aircraft body with 3D printed plate. [5]

The results of this test were positive. Saab found no visible structural damage after the test flight, which has positive implications for this field . Saab is currently looking into better material choices that have increased flexibility and temperature resistance, however; the Nylon PA2200 was able to withstand flight conditions. This material has comparable properties to PLA, making it a great example of what is possible in this field. Below is a table of important properties for both materials.

Property	PLA	Nylon PA2200
Tensile Strength (MPa)	59	48
Modulus of Elasticity (MPa)	3500	1500
Density (kg/m^3)	1250	930
Melting temperature (Celsius)	170-180	176

Table 1. PLA vs PA2200 Key Properties.

King [6] describes the existing methods of autonomous space servicing and several different robotic systems all designed to carry out various tasks on space stations and satellites. All of the robotic systems described are designed to transport, maneuver, or assemble various objects and payloads [6]. However, none are capable of conducting basic repairs to damaged components. The use of robotics for space servicing is already prevalent, but there is a lack of research and development into a robotic system that could repair, for example, damage caused by impact with small pieces of space debris. Such a system could decrease the need for astronauts to risk performing extravehicular activity for basic repairs and may increase the lifespan of satellites and space stations.

In addition to spaceflight, another application that this research more actively investigates is the potential for repairs on aircraft and vehicles utilizing a carbon-fiber reinforced PLA. If the original manufacturing involved a specific layup sequence, these patterns can be replicated in the repair. These composites are chosen in these applications because of their high stiffness-to-weight ratio that is required for flight [4]. They may also be further optimized by modifying the orientations of layers relative to each other to increase the material strength in additional directions [4]. Aircraft undergo damage throughout their life and experience 972 damages to composites per one million flight hours on average [4]. In our research, we will test



the material properties of specimens with 3D printed repairs of various lay-up sequences with PLA to determine the potential for this technology.

In the following sections, we discuss literature related to the aspects of the project that require immediate attention for implementation. This includes the materials in question, the slicing and gcode required to print our specimen, and existing work regarding infill patterns.

2.2 Materials

For the purpose of our project, we will be testing our in situ repairs using PLA and ABS filament. These materials are inexpensive compared to other popular filaments and are proven to work well with the printer we are using, the Ender 3 Pro. This section discusses the physical properties and applications of each filament, and compares the two.

2.2.1 PLA

Polylactic acid (PLA) is a common filament used for 3D printing due to its high strength and low cost of \$20-\$30/ per kilogram compared to similar filaments [7]. It is one of the world's most researched 3D printed materials, and has proven applications in bio-printing, rapid manufacturing, construction and home development, and more.

Although PLA has a tensile strength of 59 MPa and an elastic modulus of 3500 MPa, it is a very brittle material. PLA exhibits 5-7% elongation at break, according to researchers at MIT [7]. Furthermore, it has poor heat resistance properties. This limits its applications to those that do not require plastic deformation at high stress levels or extreme temperature ranges.

Despite the brittleness and poor thermal resistance properties of PLA, it is actively used in the medical field. Specific applications in this area vary and range from being used for stents

and screws in surgery to soft-tissue implants and tissue engineering scaffolds [7]. Another set of MIT researchers, Shady Farah and Daniel Anderson, analyzed the mechanical properties of PLA and their functions in everyday applications. They looked at how PLA is used in the medical field and what considerations are needed when selecting a filament. Since PLA boasts unique characteristics such as biodegradability and eco-friendliness, it is a prime candidate for these applications. Farah and Anderson cite that properties such as flexural modulus, tensile strength, and elongation are all critical criteria to consider when using PLA [7].

Physical properties of PLA are well documented in existing literature, but there are still some important properties that are worth noting. See Table 1 for key figures.

2.2.2 ABS

Acrylonitrile Butadiene Styrene (ABS) is another common filament used in FFF printing. ABS has high impact strength and a working temperature range of -30 Celsius to +60 Celsius, so it can be used in harsh environments [8]. According to researchers at Omnexus, ABS can withstand up to a maximum 50% elongation at break, which characterizes ABS as a relatively ductile material in FFF printing. A summary of other important physical properties can be found below in Table 2.

Property	ABS
Tensile Strength (MPa)	44
Modulus of Elasticity (MPa)	3500
Density (kg/m ³)	1070
Melting temperature (Celsius)	170-180

Table 2. ABS Key Properties

One of the most common applications of ABS is in piping systems. The polymer can endure long term heat exposure with relatively small change to its physical properties, making it suitable for many types of fluids, hot or cold [9]. Another perk of this filament is it's abrasion and chemical resistance. It is very chemically resistant and can withstand corrosive environments [9]. Specifically, in gravity flow piping systems, the abrasion resistance enables long-term low surface roughness. This leads to a slope reduction in the piping and can reduce building height and cost [9]. In some cases, ABS pipes are favored over stainless steel because of these factors.

2.2.3 Comparison

Researchers at the University of Manchester subjected five common FFF filaments to a three-point bending test. Their results show that PLA is 77% stronger than ABS in this type of environment [10]. Our project aims to build off of this research by using a three-point bend test to determine the strength of various infill patterns and infill percentage combinations of a repaired specimen. The bar graph below shows the Bending modulus for PLA, ABS, and their different carbon fiber variations. Reinforcing filaments with carbon fiber is known to increase the strength of the material [10].

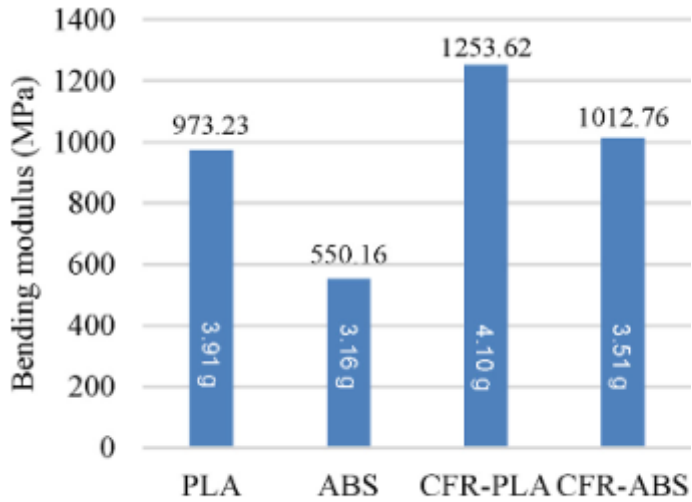


Figure 3. Bending Modulus bar graph of different filaments. [10]

2.3 Slicing and Gcode

Challenges facing conformal additive manufacturing are related to material properties and the algorithm used to generate the toolpath. Rheological properties play a key role in creating layers accurately for both planar and freeform processes in addition to printing speed, curing time and gap height. [11] talks about the printing algorithms that were developed and used to build 3D structures on freeform substrates.

The printing head in extrusion-based 3D printing moves according to tool path data points distributed in the Cartesian space (i.e., the x, y, and z axes). In planar 3D printing, a filament is deposited in the x–y plane within the same layer, while the z-value is constant in each layer with an amount equal to the desired layer thickness. In contrast, for conformal 3D printing, the z-value changes dynamically with x–y values within the same layer according to the shape of the freeform substrate. Toolpath planning depends on the perimeters and the fill pattern defined for each layer. Thus steps must be taken to generate toolpaths for direct printing in a single layer.

2.4 Existing Work regarding Infill Patterns

2.4.1 Optimal Print Settings

In order to maximize the durability of our repaired parts, it is beneficial to have the optimal print settings for our tests.

Researchers at the University of Manchester conducted a study to find the optimal modeling parameters for FDM printing using pure PLA filament. They varied infill pattern, infill density, infill speed, and nozzle temperature. The researchers analyzed the data using a combination of tensile and compression testing, as well as scanning electron microscopy (SEM) to reach a conclusive set of optimal printing parameters [10]. Their findings showed that a linear infill pattern, 100% infill density, 90mm/s infill speed, and 215 degrees Celsius nozzle temperature were most effective for maximizing the Young's Modulus of PLA 3D printed parts under tension and compression loadings. The maximum Young's Modulus the researchers recorded for PLA was 1538 MPa [10].

Similar to the researchers at the University of Manchester, Tanner Harpool, a thesis candidate at Wichita State University, investigated the effects of infill patterns on tensile strength properties of 3D printed parts. He analyzed four different infill patterns: rectilinear, diamond, hexagonal, and solid (the control). He found that the hexagonal pattern had the highest strength. Harpool also noticed that prints with 100% infill behaved like brittle materials, which actually decreased their strength. Parts with a lower infill percentage experienced behavior more closely resembling a ductile material [12].

Another important aspect to consider in this project is the adhesion between the base part and the infill repair. In the study mentioned above, the researchers used SEM technology to reveal that the strength of the samples is dependent on the arrangement of their layers [10]. This tells us it is worthwhile to pursue the optimal infill pattern for 3D printed repairs because the orientation and layout of the filament along the 3D printed base will most likely have an effect on the overall strength of the repaired part.

There is some correlation between these parameters. For example, researchers found that increasing the nozzle temperature leads to an increase in strength; however, at a certain point, the increase in temperature becomes detrimental [10]. If the temperature is too high, it can lead to poor layer bonding, which does more harm than good. It is important to note that the change in one parameter may have an adverse effect on another parameter. In our case, we are varying the infill pattern and infill density of our repaired print. By varying the infill pattern, we may also alter the adhesion between the filament layers, and it is something that needs to be noted during data analysis.

Researchers from the University of Malaysia Perlis did further research into both the tensile and flexural strength of parts 3D printed from [13]. Their tests consisted of comparing the infill patterns used when creating the parts to compare their ultimate strengths from tensile and flexural tests. Their testing found that the rectilinear infill pattern resulted in the highest flexural and tensile strength followed by the honeycomb, concentric and hilbert curve patterns. Researchers from Shanghai University did similar testing on PLA parts by varying raster angle, layer height, and raster [14]. The flexural strength of each PLA part was found for varying combinations of each of the 3 experimental variables. Their results found that flexural strength

decreased as raster angle, and layer height while increasing with raster width until 600 micrometers before it started decreasing.

2.4.2 Structural Analysis

Existing research on structural analysis of 3D printed parts focuses on either tensile or flexural testing. For 3D printed parts, to compare different printing parameters, researchers have used tensile and flexural tests detailed in the ASTM D638-14 and ASTM D790-10 standards. The goals of the ASTM D638-14 and ASTM D790-10 are to test the tensile and flexural properties of plastics respectively. The ASTM D790-10 standard details a 3 point bending test on a given specimen. The test requires a span to depth ratio of 16:1 and for the test to continue until the part breaks or the specimen reaches 5% strain. This test also requires at least 5 specimens for a given combination of parameters to ensure proper results. To calculate the flexural strength

$$\sigma_f = \frac{3PL}{2bd^2}$$

Equation 1.

from the force measured during the test, the following equation was used where P is the load, L

$$D = \frac{rL^2}{6d}$$

Equation 2.

is the support span, b is the width of the specimen and d is the depth of the specimen. The standard defines the midspan deflection with the following equation where r is the strain. The flexural strain is defined as the following equation where D is the maximum deflection.

The modulus of elasticity was defined as the following equation where m is the slope of the initial line of the load deflection curve.

$$\varepsilon_f = 6Dd/L^2$$

$$E_B = L^3m/4bd^3$$

Equation 3.

Of these calculations detailed in the ASTM standard, the most commonly used metric for comparing different parameters was the ultimate strength of the printed part. The ultimate strength is the maximum stress the specimen experiences as it undergoes the test. With common specimen designs, this metric allows a direct comparison between different parameters to find optimal conditions. Because of this, ultimate strength is found and compared while doing structural analysis of 3D printed parts.

2.4.3 Cost Analysis

Researchers at the department of mechanical and industrial engineering at Youngstown State University investigated the relationship between infill print design and production cost-time of 3D printed ABS parts. This relationship is extremely important to consider in our research, because while users would want to select the infill print pattern that provides them with the best strength retention, they also need to review production costs associated with each infill pattern. Selection of an infill pattern can significantly affect mechanical properties, total cost, and production time [15].

The researchers printed multiple specimens of four different infill patterns: low density, high density, double dense, and solid infill. The prints were subject to ASTM standards, which are the same standards we are using in this project. Once printed, the researchers tested the tensile, compressive, and bending strength of each infill pattern. To calculate the total cost of each print, they estimated the cost per minute of printing ABS on their print setup, then multiplied this by the time it took to print the sample [15]. Certain infill patterns will contain more material, which leads to higher costs; furthermore, the toolpath the extruder head takes for complex infill patterns can also increase the print time. These are all factors that need to be accounted for in a cost-benefit analysis. In a practical cost-benefit analysis, situation is everything. For a Mars Rover, the extra cost associated with a stronger repaired piece may be well worth it. On the other hand, in a mass production application, cost would likely be the driving factor.

The Youngstown State University researchers found that in order to obtain a greater cost reduction, the user needs to take a hit in the mechanical strength. However, the data shows that although the low density piece had a very similar modulus (MPa) to the high density piece in bending tests, the low density piece had a much better cost savings when compared to the solid infill piece. The low density had modulus 456.68 MPa, while the high density piece had modulus 459.83 MPa. The cost savings of the low density infill when compared to the solid piece was close to 4%, and it actually cost 3.5% more to print the high density infill piece. The researchers suggest additional analysis on more complex infill patterns [15].

Chapter 3: Methodology

3.1 Background and Reasoning

3.1.1 Background

Upon completing our initial setup of the printers, we moved into creating a procedure and establishing standards for printing pieces we were interested in. Beginning with a layer height of 0.2 mm (the standard layer height for a 0.4 mm extruder head) and a 20% infill, we initially ran into problems with layer separation. This is caused by a lack of adhesion between two layers in a print that results in a slight gap that compromises the structural integrity of the piece. To remedy this issue, we adjusted the layer height to 0.12 mm. After finalizing the layer height, we increased the percent infill to 100%, since this would be the maximum infill we would use throughout our trials. While testing this, a common issue we faced was warping. The temperature of the bed is controlled and held constant during the printing process by the printer itself. The temperature of the PLA, however, cannot be directly controlled, so any plastic not in direct contact with the bed cools down and therefore contracts. This can result in deforming along the bottom of the print which compromises its structural integrity. To combat this problem, we insulated the printer using cardboard, closed any windows in the printing room(to prevent drafts), and used hairspray on the print bed to keep the print attached to it. After these modifications, we had great success with printing pieces similar to that of our damaged pieces and began our specimen testing. Using a separate model for the infill piece, we successfully printed in the hold to repair it. The progression of these results is shown in the figure below.

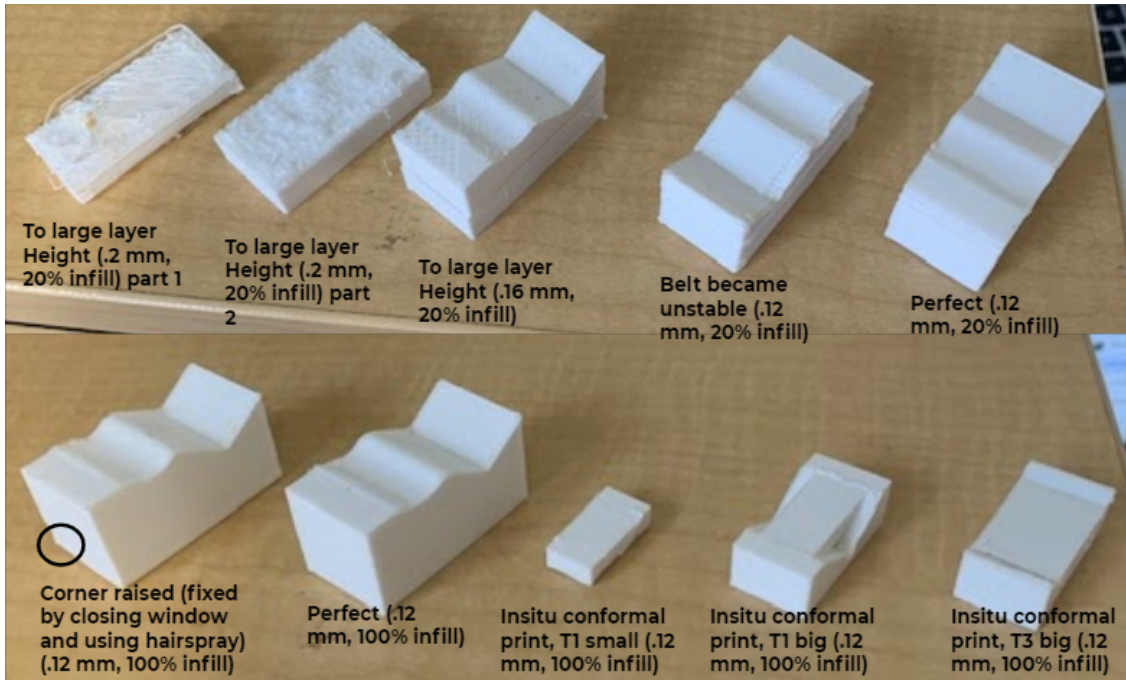


Figure X. Progression of initial prints

3.1.2 Reasoning

One of the main objectives of our research was to determine the most efficient infill pattern and infill percentage combination for repairing a damaged 3D printed part. Efficiency in our case is defined as the strength of the repaired piece to the time it took to repair the damaged section. We printed the test specimens as rectangular beams for simplicity and easier data analysis. Printing in this configuration allowed for multiple variations of the simulated damage section. Specifically, our main simulated damage section was an inverted triangular prism, which we denoted T1 (figure number). Our secondary simulated damaged section was a semispherical void, denoted as T4 (figure number). The specimens comply with common practice ASTM standards, which are discussed further in section 3.3.

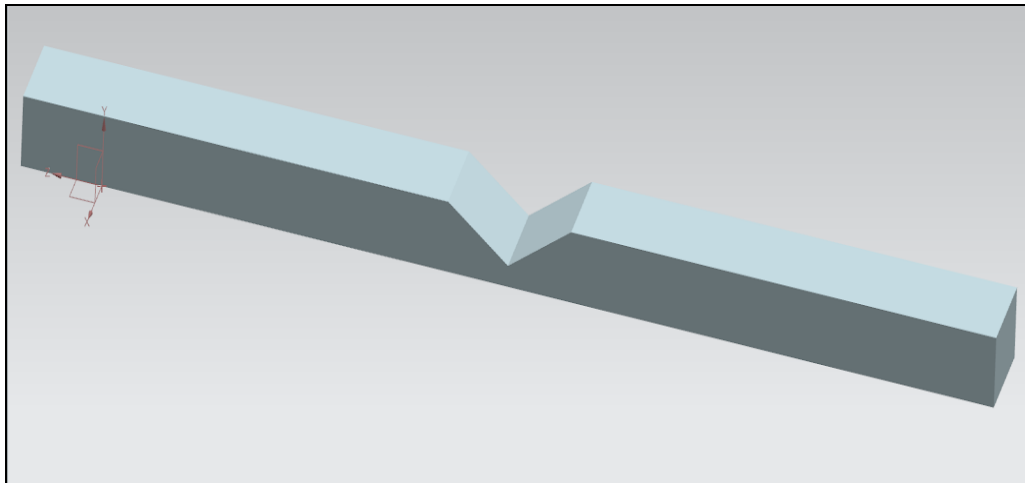


Figure X. T1 damaged specimen without repair

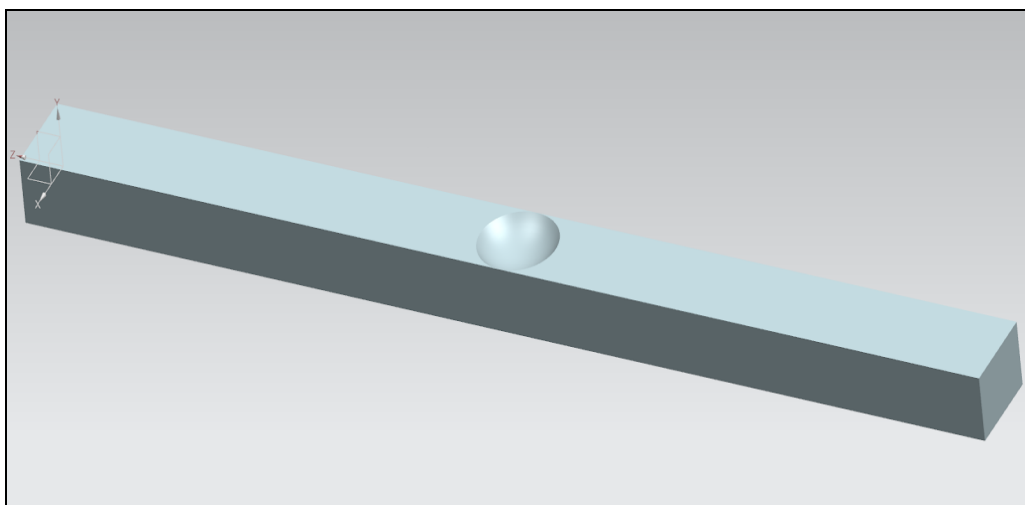


Figure X. T4 damaged specimen without repair

The voids were chosen as a proof of concept for the ability to repair two completely different types of damage. Due to limitations with the dimensions of the nozzle we used, the maximum angle that we could print on was 45 degrees above the horizontal. As a result, the voids chosen could not at any point require printing on a surface above 45 degrees. The T1 and T4 void geometries were selected to mimic simplistic slice and circular imprint damages respectively while also meeting the angle requirements. In addition, the simplicity of both voids allowed for easier calculations regarding the stress and strain each piece was undergoing.

We determined the best method to evaluate the strength of a repaired piece was a 3-point bend test. This test is one of the most commonly used tests for collecting stress versus strain data for a structure, and was abundant in the literature related to our project. It is known for its ease of specimen preparation and testing. Another common method to collect stress versus strain data is a tensile strength test; however, we decided that for the possible applications of repairing a damaged 3D printed structure, the loads the specimen experiences would most closely be represented by a 3-point bend test.

3.2 Hypothesis(es)

The goal of this research was to test whether a damaged 3D printed structure could be repaired using conformal printing methods so that the strength of the structure after the repair would not be significantly lower than the strength of the original undamaged structure. Since our research aims to be a small-scale proof of concept, we predicted that we could vary the design and settings of the printed repairs in order to maximize the strength of the repaired structure and achieve the ultimate strength of an undamaged piece.

As discussed in section 3.1, we developed designs for two different types of damage that we could repair and test. When considering other potential variables for the experimentation process, we decided to analyze two main factors: infill percentage and infill pattern. In order to find the optimal infill percentages, we conducted tests with 20%, 40%, 60%, 80%, and 100% infill. We predicted that an infill percentage of 100% would yield the strongest repair; however, we also predicted the 100% infill would also have the highest material cost and the longest print duration. To vary the infill pattern, we conducted repairs using the rectilinear, hexagonal, and aligned infill patterns. Figure X below provides a visual comparison of the infill patterns.

According to a study conducted at the University Malaysia Perlis, the rectilinear pattern displayed the highest tensile strength when compared to more complex infill patterns such as honeycomb and concentric, so we determined that rectilinear would likely be the strongest in our experiment [1].

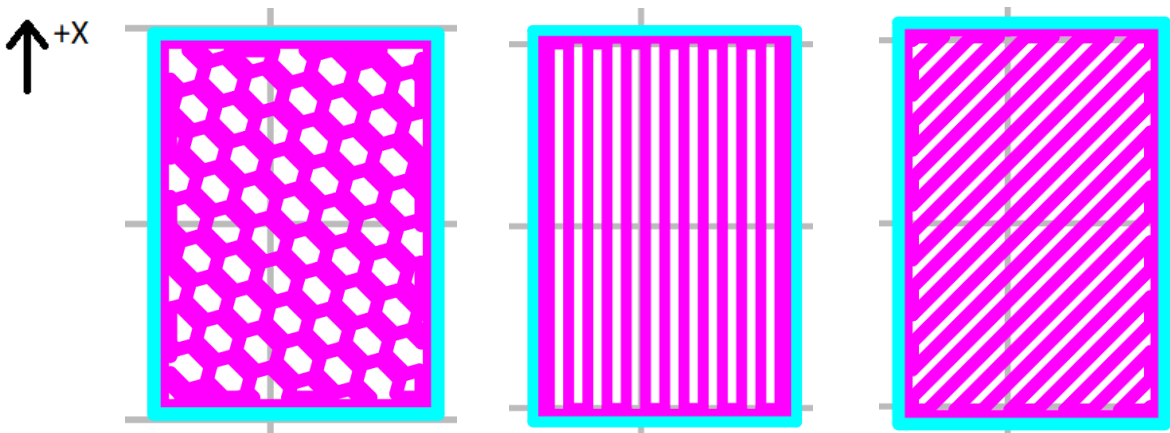


Figure X. Different infill patterns. From left to right: Hexagonal, aligned, rectilinear

Although our project focused solely on conducting 3D printed repairs using fused deposition modeling (FDM), we believe that the methods we developed and tested could be modified and applied to other types of 3D printing as well in future studies.

[1] S. F. Khan, H. Zakaria, Y. L. Chong, M. A. M. Saad, and K. Basaruddin, “Effect of infill on tensile and flexural strength of 3D printed PLA parts,” *IOP Conference Series: Materials Science and Engineering*, vol. 429, p. 012101, Nov. 2018, doi:10.1088/1757-899x/429/1/012101.

3.3 Testing Standards

For the experimentation process, we adhered to the ASTM standards for testing the tensile properties of plastics. These standards determined the overall dimensions of our printed pieces and the number of pieces to be tested for each category. ASTM requires 5 parts to be

tested for each variable, so we chose to print and test 6 pieces for each type of infill percentage and pattern in order to be more thorough [2]. We also used ASTM standards to determine the dimensions of the printed test pieces. The requirements for bend testing of plastic parts included a 16:1 span to depth ratio for each design. In addition, each end needed to have an overhang length that was 10% of the span when mounted in the testing setup [2]. As a result, each of our pieces was 19.2 cm long with a 1cm depth and 1.5cm width.

The standards we used to determine these dimensions were intended for rectangular plastic test pieces. For the purpose of our study, we used rectangular prisms with designed damage as shown in section 3.1.2. These pieces were not precisely rectangular due to the repaired damage, but the overall designs were approximate rectangular prisms so we chose to use these standards for all experiments.

[2] “Standard Test methods for flexural properties of unreinforced and reinforced plastics and electrical insulating materials,” *Annual Book of ASTM Standards*, vol. 8, no. 1, 2017.

3.4 Materials & Equipment

3.4.1 Printer

To print all specified pieces we purchased four Ender 3 Pro 3D printers. The printers were assembled, operated, and housed by team members. The Ender 3 Pro was chosen due to it being inexpensive, easy to operate, and having a large enough print bed. Four of them were purchased in order to print the large number of pieces required within our planned timeline.

The overall geometries, damage void geometries, infill percentages, and infill patterns we used for our various test specimens have been discussed in sections 3.1 - 3.3. In addition to these test variables, we also conducted several rounds of testing with pieces made out of acrylonitrile

butadiene styrene (ABS) plastic, another commonly used material in FDM additive manufacturing other than PLA. The purpose of testing with other materials was to see whether our results and conclusions were specific to PLA, or if there is reason to believe they are applicable to FDM in general.

3.4.2 Testing Equipment

We had initially planned on utilizing equipment available on the University of Maryland campus to perform 3-point bend tests and collect data. However, the COVID-19 pandemic had begun shutting down campuses across the country just prior to the start of our planned data collection. To ensure that we would be able to continue collecting data regardless of pandemic procedures, we decided to construct our own testing/data collection apparatus that would remain in and be operated from our own homes.

To perform 3-point bend tests, we used a Mophorn 6 ton H-frame hydraulic shop press. This is a hand-operated press that works by pumping a lever. A load cell that measured the force being applied by the press was attached to the press using cold-weld steel epoxy. Other types of presses were considered such as more expensive models with built-in load cells and electronic actuators. There were two reasons why we chose the simpler, hand-operated press. The first was budgetary constraints. One of those higher-end models would have taken up the majority of our overall budget, leaving little room for printers and other supplies. By building our own testing apparatus with the simpler press, we were able not only to have multiple test setups but also to allocate much more of the budget for printers and printing materials. This proved to be incredibly helpful as the time required to print and test all of the samples was a significant constraint. The other reason for choosing the simpler press was for the learning value of the experience. While not related to the empirical results of this study, we believe that the process of designing and

fabricating our own testing apparatus provided us with valuable experience in engineering, design, and troubleshooting. This also allowed us to become more familiar with the standards and methods for testing in 3-point bending, giving us a better understanding of the procedures involved in testing and analyzing the results.

In addition to the press itself, the test pieces were supported by two steel plates on either end which were clamped to the frame of the press. The steel plates also needed to be raised a few centimeters so that the pieces had room to be bent to failure. To do this, steel hex bolts were placed under the corners of each steel plate. At the edge of each steel plate and on the bottom of the load cell are $\frac{1}{4}$ " diameter stainless steel D-shafts with the flat sides attached with epoxy to the plates and load cell respectively. This was to make sure that all the forces applied to the test piece were each being applied at a single point to allow for easier and more accurate structural analysis. The end supports were positioned 16 cm apart, with the load cell midway between.



Figure X. Overall Testing Apparatus



Figure X: Zoomed-in picture of how the test piece was positioned

Data collection was performed using an Arduino Uno microcontroller, a 200kg S-type load cell, and 350-ohm resistance strain gauges. The load cell was wired to the Arduino with an HX711 load cell amplifier, and could measure the applied force directly. To measure strain, the strain gauge was set up in a Wheatstone bridge circuit with three other resistors as in the figure below. A Wheatstone bridge is used for sensing strain by detecting small changes in voltage across the resistors corresponding to changes in resistance of the strain gauge. The Wheatstone bridge was also connected to the Arduino via an HX711 load cell amplifier. Figure 4 below is a diagram of the circuit we used to take data.

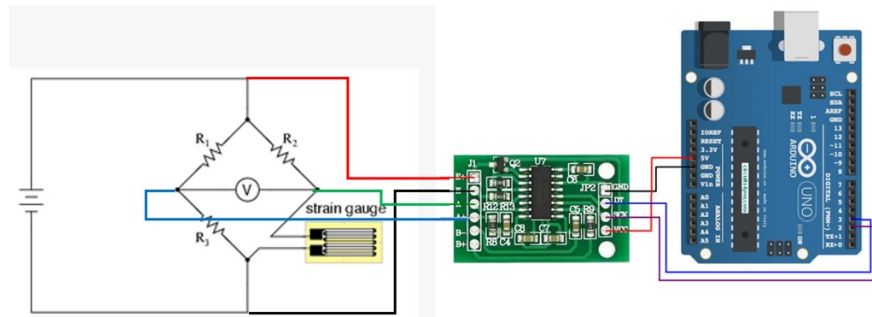


Figure 4. Wheatstone bridge, HX711, and Arduino circuit diagram

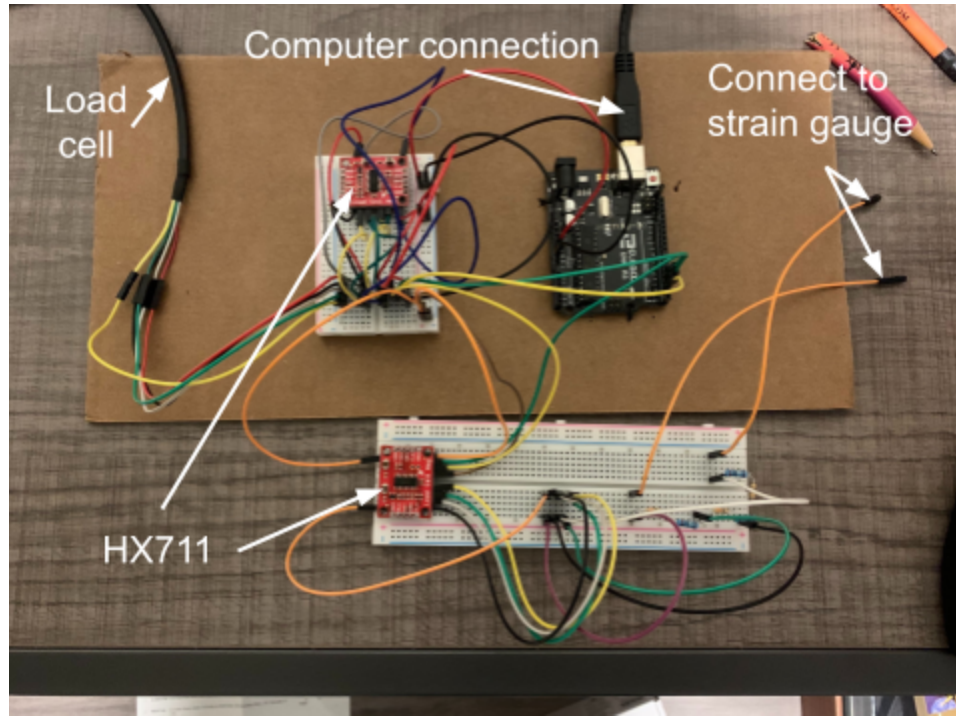


Figure X. Complete circuit

Our Arduino code read in data from the load cell and strain gauge and outputted values of force in kg (converted to Newtons by multiplying by $g = 9.8 \text{ m/s}^2$) and millistrain. An additional program written in Processing outputted the data to a csv file format.

3.5 Experiment/Steps Taken

3.5.1 Experimentation Design

Control	
Undamaged	Damaged
6 parts printed at 100% with no damage or repairs	6 parts printed with T1 damage

The first tests completed were control pieces of PLA 3D printed at 100% infill with full rectangular geometry (no damage, no repair). [add picture] These pieces represented the undamaged structure, and so would be the baseline to which all other testing would be compared.

To evaluate the quality of a repair, we wanted to compare ultimate stress and stress vs strain curves between undamaged, damaged, and repaired pieces for a given infill and type of loading (different types of loading are discussed below). These pieces were also used to practice the test procedure and determine the proper testing method (described further below). Using the load cell, the force applied to the part was measured in kilograms and used to calculate the ultimate strength of the part before failure. The strain of the part was measured in millistrains to ideally note strain at the point of failure. The units of kilograms and millistrains were chosen because those were the units listed in the documentation that came with the sensors.

Control testing was followed by testing of the T1 damaged geometry. The results of this testing were meant to show how much the overall strength of the piece was impacted by a small area of simulated damage. Once again, they would also be compared to the results of the repair testing so we could quantify the impact of the repair on the strength of the overall piece.

Infill Testing	
Infill of repair	T1 Geometry
20%	6 parts
40%	6 parts
60%	6 parts
80%	6 parts
100%	6 parts

The infills used for repairs were 20, 40, 60, 80, and 100% while the damaged initial part was kept at 100% for all tests. [<- picture explaining this] We wanted to test various infills for the repair to determine which infill would give the maximum strength and if there was an optimum point for strength vs material cost.

Control	
Undamaged	Damaged
6 parts printed at 100% with no damage or repairs	6 parts printed with T1 damage
	12 parts printed with T4 damage (6 compression, 6 tension)

After initial infill testing, we wanted to corroborate our results with those of a different damage geometry. Real-life damage comes in an infinite number of sizes and irregular shapes, so to prove that our results are applicable to some general damage with our limited time and resources, we conducted damaged and repaired testing for the T4 geometry which has rounded instead of flat faces and has a smaller void volume. Our goal here was to be able to show similar trends in the analysis of the results between the T1 and T4 geometries. We also kept in mind though that seeing differing trends for the different damage geometries would also be useful information.

Tension Vs. Compression	
T1	T4
6 parts printed with conformal repairs facing down at 100% infill (Tension)	6 parts printed with conformal repairs facing down at 100% infill (Tension)
6 parts printed with conformal repairs facing up at 100% infill (Compression)	6 parts printed with conformal repairs facing up at 100% infill (Compression)

The nature of a structure in bending is that one side of the structure is in tension while the other is in compression. We wanted to analyze results for the damaged and repaired sections in both types of loading. Therefore, damaged and repaired pieces were tested with the void/repair either on top of the beam (compression) or on the bottom (tension). The T1 damage geometry did not allow us to test these pieces with the void in compression because the applied force would have been in the void and hence at an angle (figure X.), so a basic 3-point bend analysis would not have been appropriate. T4 damaged pieces could be tested in compression because the void did not span the entire width of the piece (figure X.). Data for both tension and compression were collected for all other pieces.

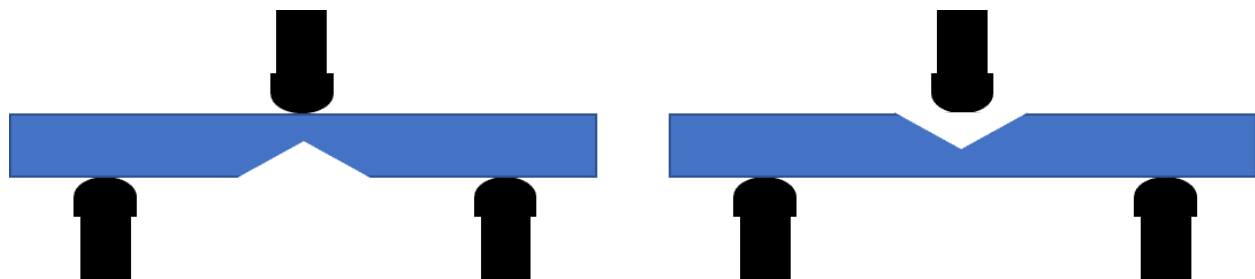


Figure X: T1 damaged tension testing (Left), T1 damaged compression testing (Right).

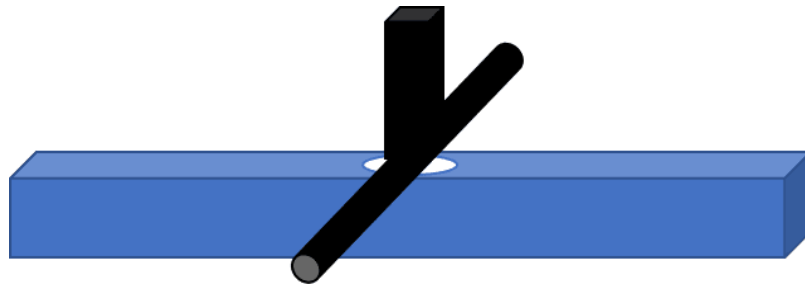


Figure X: T4 damaged compression testing

Infill Pattern	
Hexagonal	Aligned
12 T1 parts printed at 40% infill (6 compression, 6 tension)	12 T1 parts printed at 40% infill (6 compression, 6 tension)
12 T1 parts printed at 60% infil (6 compression, 6 tension)	12T1 parts printed at 60% infill (6 compression, 6 tension)
12T1 parts printed at 80% infill (6 compression, 6 tension)	12 T1 parts printed at 80% infill (6 compression, 6 tension)

The infill pattern used for all testing up to this point was rectilinear. To obtain more comprehensive results, we wanted to vary this as well. The same undamaged (control) and damaged pieces were used as before, and only the infill of the repair itself was varied. The other infill patterns tested were aligned and hexagonal [Figure X. Different infill patterns], and once again the infill percentage was varied between 20, 40, 60, and 80%. (100% infill was not

included here because our slicing software and printers were only capable of printing 100% infill in a rectilinear pattern). Once again, results were obtained for both tension and compression.

Finally, to corroborate our findings and again show that they are applicable to a wider range of cases, we performed T1 infill percentage testing using ABS. Just as when we tested the different damage geometries, we hoped to see similar trends in the analysis between the different materials, but differing behaviors would still be important and useful information.

3.5.2 Printer Setup

To maintain consistency throughout the experimentation process, we used the Ender Pro 3 with a 0.4mm nozzle and identical settings for each set of prints.

The nozzle and printer bed temperature settings were dependent on the material being used. For PLA prints, the nozzle temperature was set to 200°C and the bed temperature was 70°C. For ABS prints, the nozzle temperature was set to 200°C and the bed was set to 95°C.

In addition, we sprayed a thin layer of hairspray to the printer bed immediately before each piece began printing. This was done to ensure that the first few layers of the print properly adhered to the surface of the bed. Without this step, the initial layers had a tendency to slide across the printer bed, causing the print to fail. In some cases, we found that it was also beneficial to preheat the printer bed for 15-20 minutes before starting the actual print. This also improved adhesion to the bed at times when the room temperature was colder than usual; for example, during the winter months or even when the air conditioning in the room was set to a lower temperature.

3.5.3 Printing Procedure

The step-by-step procedure used for printing each of the samples is as follows.

Step 1) Preheat the nozzle and bed to specified temperatures as outlined above in section 3.5.2.

Step 2) Spray the bed of the 3D printer with hair spray in order to minimize the chance of warping along the edges of the piece. The hairspray added a layer of adhesion between the print bed and the piece being printed. For the purposes of our printing, Suave max hold unscented hairspray was used.

Step 3) If warping continued to be an issue, insulate the 3D printer. This prevents drafts and rapid changes in temperature from causing warping or other complications in our prints. We insulated the printers using cardboard boxes. Figure X below shows the following set up.



Figure X: Insulation of print bed using cardboard

Step 4) Print the base piece. The base piece for every repaired test was a rectangular prism (of dimensions described in Section 3.3: Testing Standards) at 100% infill, with either a T1 or T4 hole in the center of it.

Step 5) Wait at least one hour to allow for the temperature of the nozzle, bed, and PLA to return to standard conditions.

Step 6) Begin stopwatch. Print in the designated damage of the base piece with a piece of correct proportions to fully fill the hole. Once damage has been completely repaired, stop the stopwatch and record time. For the fill piece, we would vary its infill pattern and infill percentage to what was being tested.

3.5.4 Testing Procedure

The step-by-step procedure used for testing each of the samples is as follows.

Step 1) Attach the strain gauge. The strain gauges were attached using super glue onto the underside of each test piece directly underneath the point of applied force (in the middle). A small drop of super glue was applied to the test piece after wiping it clean of any dirt and dust. The strain gauge was then gently applied and the test piece set aside for the glue to sufficiently dry. The strain gauge was placed in the middle so that it would be located at the point of maximum strain and on the underside so that it wouldn't be crushed by the press. This, however, meant that a few of our test geometries could not be tested with a strain gauge applied. When any of the "damaged" pieces, either T1 or T4, were tested in tension (with the void on the bottom), the location that the strain gauge would need to be was exactly where the void in the piece was. Therefore there was no strain data collected for any of the damaged pieces in tension, and analysis was done just using load/stress data.

Step 2) Solder wires onto the strain gauge. Some strain gauges are available with lead wires already attached, however the ones we used did not, and so wires had to be soldered on. The strain gauges are both very small and very fragile, so an accidental tug on a wire could easily tear the strain gauge. Therefore, the test pieces had to be handled very carefully once the wires were attached. It was also important to make sure that the strain gauges did not overheat

while applying solder. Too much contact with the soldering iron could burn through or damage the performance of the strain gauge.

Step 3) Place the test piece in the testing apparatus. Each test piece was placed on the end supports so that the load cell was positioned directly above the midpoint, and the strain gauge wires were connected to the rest of the Wheatstone bridge circuit.

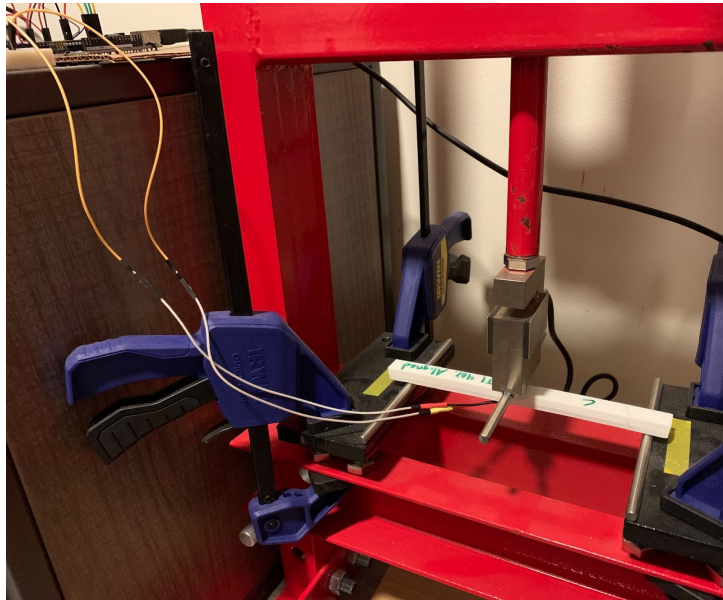


Figure X. Piece Connected to Arduino and Ready for Testing

Step 4) Run the test. After zeroing the load cell and editing the Processing code to contain the appropriate test file name, the Processing code can be run to begin data collection. When conducting 3-point bend tests, ASTM standards dictate that the piece must be bent at a rate of 5% strain per second. Since our press was hand-operated in addition to the fact that we could not read in and display strain data as the test was occurring, we were unable to strictly adhere to this standard strain rate. Instead, the press operators simply had to do their best to keep the press rate consistent between tests. Although this deviates from ASTM standards, we do not believe that it had any significant effect on the quality of our data collection or analysis, as we

were primarily interested in comparing overall stress vs strain curves as well as maximum stresses.

Each test was run until the piece reached ultimate failure. For some pieces, this was at a clear point when the piece suddenly fractured into two or the repair suddenly snapped off. Other pieces yielded but did not fracture, in which case the test was run until the press reached its maximum stroke. Running the test for longer than necessary was not an issue since the moment of yielding can be easily identified in the data. All data was recorded as csv files with columns of time, force, and strain. [REDACTED]

Chapter 4: Results

4.1 Overview

From the conducted experiments, the maximum force applied and the strain at ultimate strength was recorded. In cases where the strain gauge broke before the ultimate strength was achieved, the highest recorded strain was used. From the maximum force applied, the ultimate strength was calculated and both the maximum force and ultimate strength were used for comparison of the efficacy of each repair. Per the ASTM D790 standards, the average force and ultimate strength of the 6 tests for each case were used for the following comparisons.

4.2 Collected Data

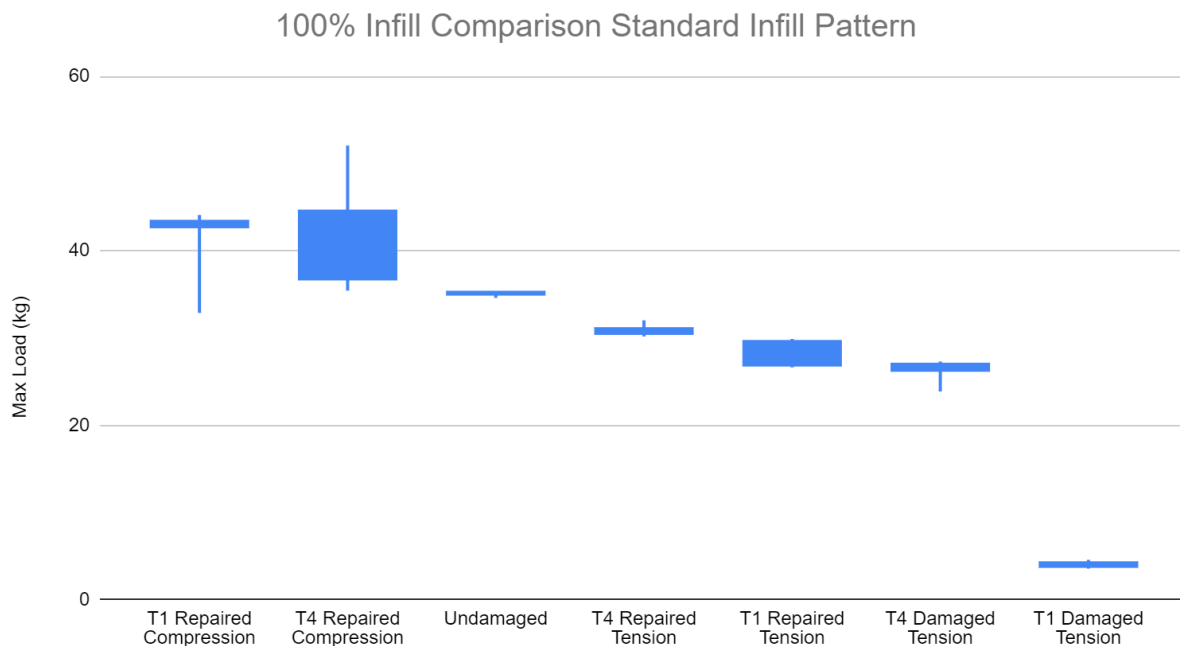


Figure X. 100% Infill Comparison Standard Infill Pattern

100% Infill Testing				
	Mean Ult. Load (kg)	Std dev. (kg)	Mean Ult. Stress (MPa)	Std dev. (MPa)
T1 Repaired Compression	43.69	7.22	68.57	11.33
T4 Repaired Compression	44.39	8.52	69.67	13.38
Undamaged	35.24	0.51	55.31	0.80
T4 Repaired Tension	31.35	1.14	49.21	1.78
T1 Repaired Tension	28.88	2.04	45.33	3.20
T4 Damaged Tension	26.52	1.41	53.41	2.83
T1 Damaged Tension	4.21	0.53	73.46	9.23

Figure X. 100% Infill Testing

T1 Infill Pattern Testing

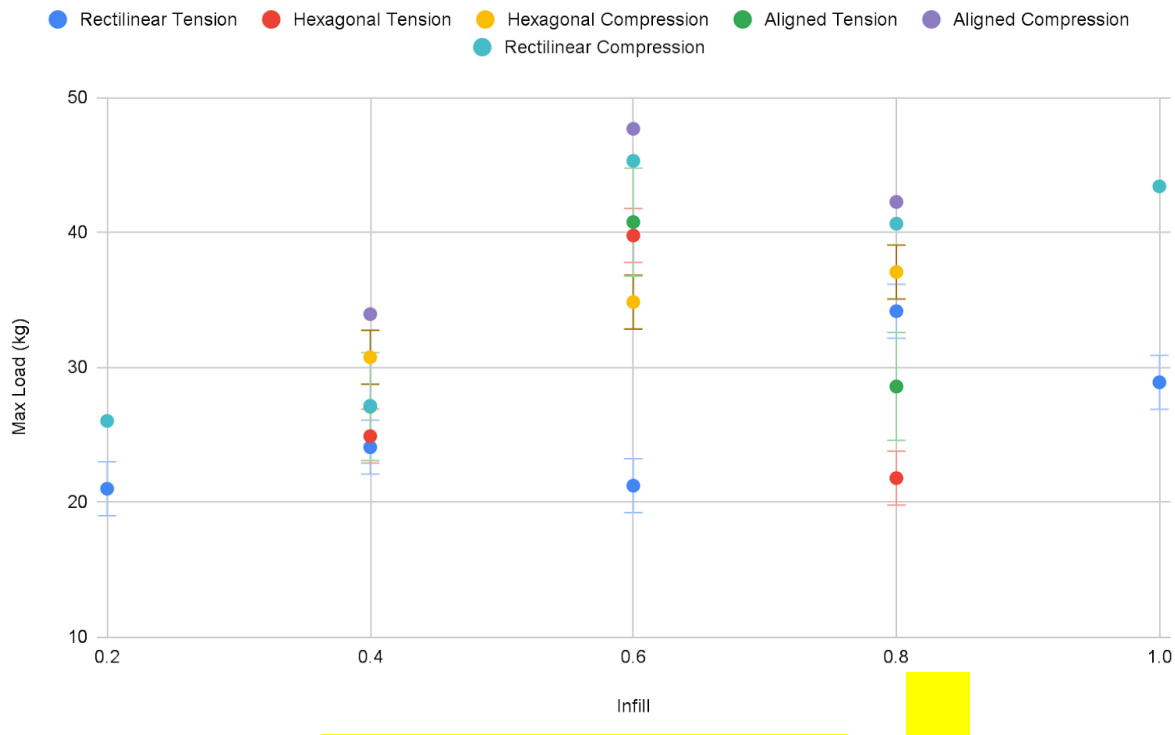
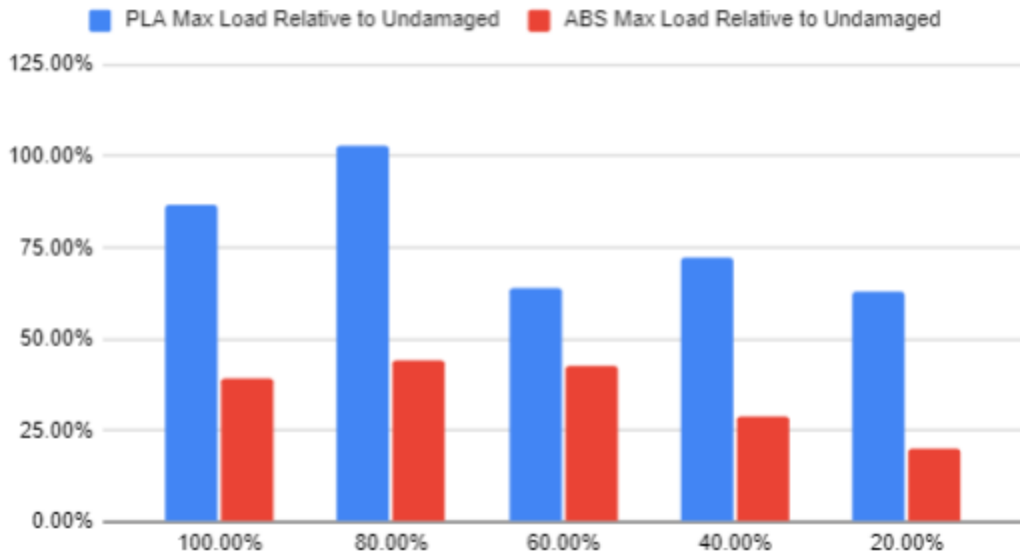


Figure X. T1 Infill Pattern Testing Graph

Infill	20%	40%	60%	80%	100%
Rectilinear Tension	20.98	24.07	21.21	34.15	28.88
Rectilinear Compression	26.01	27.13	45.30	40.63	43.41
Hexagonal Tension	-	24.89	39.76	21.77	-
Hexagonal Compression	-	30.73	34.83	37.05	-
Aligned Tension	-	27.08	40.76	28.57	-
Aligned Compression	-	33.93	47.67	42.25	-

Figure X. T1 Infill Pattern Testing Data

Strength Relative to Respective Undamaged



*Add descriptor stating rectilinear; can't contradict claim that 60% aligned is strongest

Figure X. Strength Relative to Respective Undamaged

ABS vs. PLA				
	PLA max Load (kg)	PLA Relative to Undamaged	ABS max Load (kg)	ABS Relative to Undamaged
Undamaged	33.25		27.58	
Repaired 100% Infill	28.88	86.85%	10.84	39.29%
Repaired 80% Infill	34.15	102.70%	12.22	44.30%
Repaired 60% Infill	21.21	63.79%	11.75	42.58%
Repaired 40% Infill	24.07	72.37%	7.94	28.79%
Repaired 20% Infill	20.98	63.10%	5.49	19.92%
Damaged	4.24	12.74%	1.48	5.35%

Figure X. ABS Vs PLA Testing Data

4.3 Data Analysis

4.3.1 Comparisons

For initial 100% infill testing, both the T1 and T4 geometry in compression were found to withstand a higher load than the undamaged control parts. This difference was found to be a

123.9% and 125.9% increase respectively in average max strength relative to the undamaged parts. Below the control strength, T4 and T1 repaired pieces in tension were found to have 88.9% and 81.9% average strength relative to undamaged with T4 damaged in tension following with 75.2%. The weakest part of this initial round of testing was found to be T1 damaged in tension with a relative average strength of 11.9% to undamaged.

From infill pattern testing, the highest mean strength was found from the aligned compression infill at 60%. This result was similarly found with Aligned tension, Rectilinear compression, and Hexagonal tension all having their highest strength at 60% infill. Hexagonal compression had the highest strength at 80% infill while the rectilinear tension was a clear outlier of the group with the lowest strength at 60%.

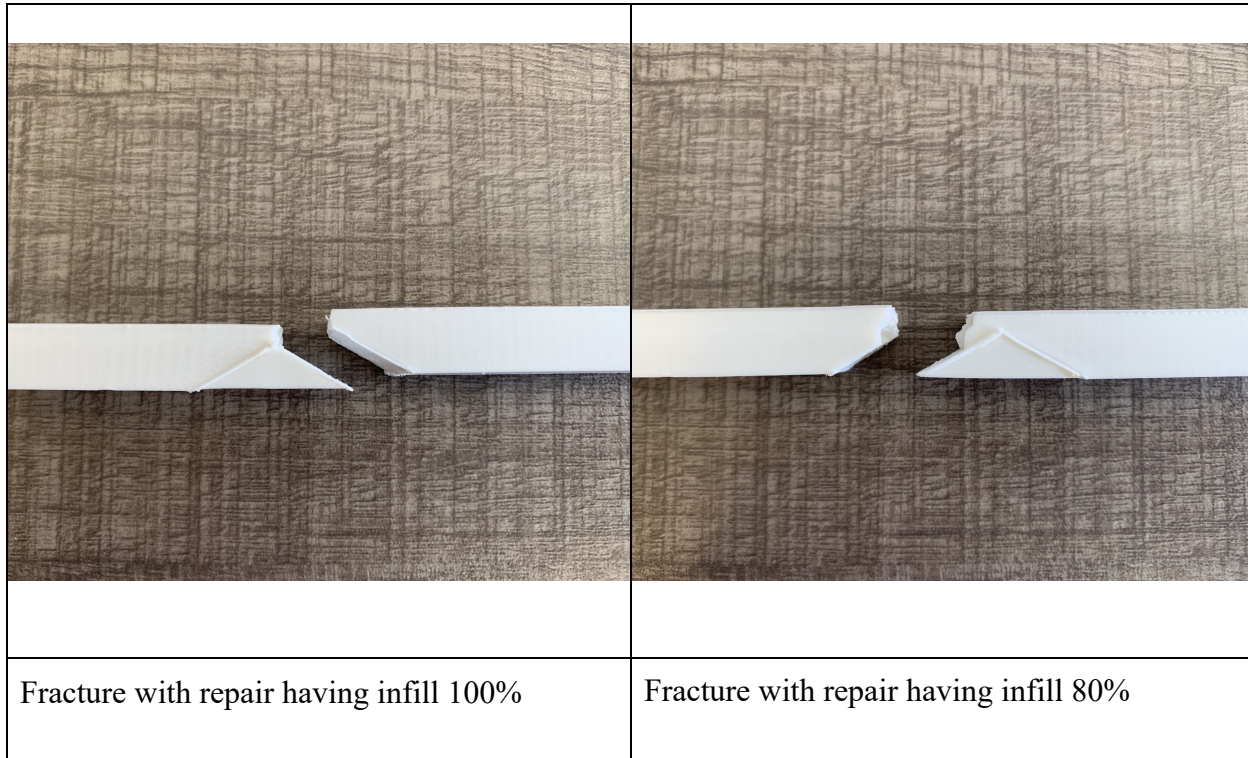
For the ABS testing in comparison to PLA, ABS was found to be much less effective in its repairs than the PLA. The closest ABS repairs were able to reach in comparison to undamaged control was 44.3% at 80% infill while PLA was able to achieve 102.7% of the undamaged ultimate strength at 80% infill.

4.3.2 Optimization

Two factors were used when determining the optimized solution: infill pattern and infill percentage. For the infill pattern, the aligned pattern compression was found to be the strongest for the 40, 60, and 80 infill percentages (T1 pattern infill testing graph). For the infill percentages, the 60 and 80 had the most outstanding results. The 60 percent infill withstood the highest load when testing with the aligned pattern tension while the rectilinear tension resulted in an obvious low outlier from the remaining 60 percent infill data. For the rectilinear and hexagonal infill patterns, the 80 percent infill yielded the best results, however they were still lower than the aligned pattern.

Overall, the geometry that gave the best results was the hexagonal pattern. This was determined through taking the difference between the damaged and repaired data of each of the infill patterns and comparing those differences. Thus, through looking at the data we collected, T1 had the largest increase with the repairs in tension and compression being 82 with a 123.2% increase in effectiveness compared to the undamaged control pieces. This conclusion was to be expected as the geometry of the hexagonal pattern is not directional as opposed to the rectilinear and aligned infill patterns.

4.4 Theoretical Analysis



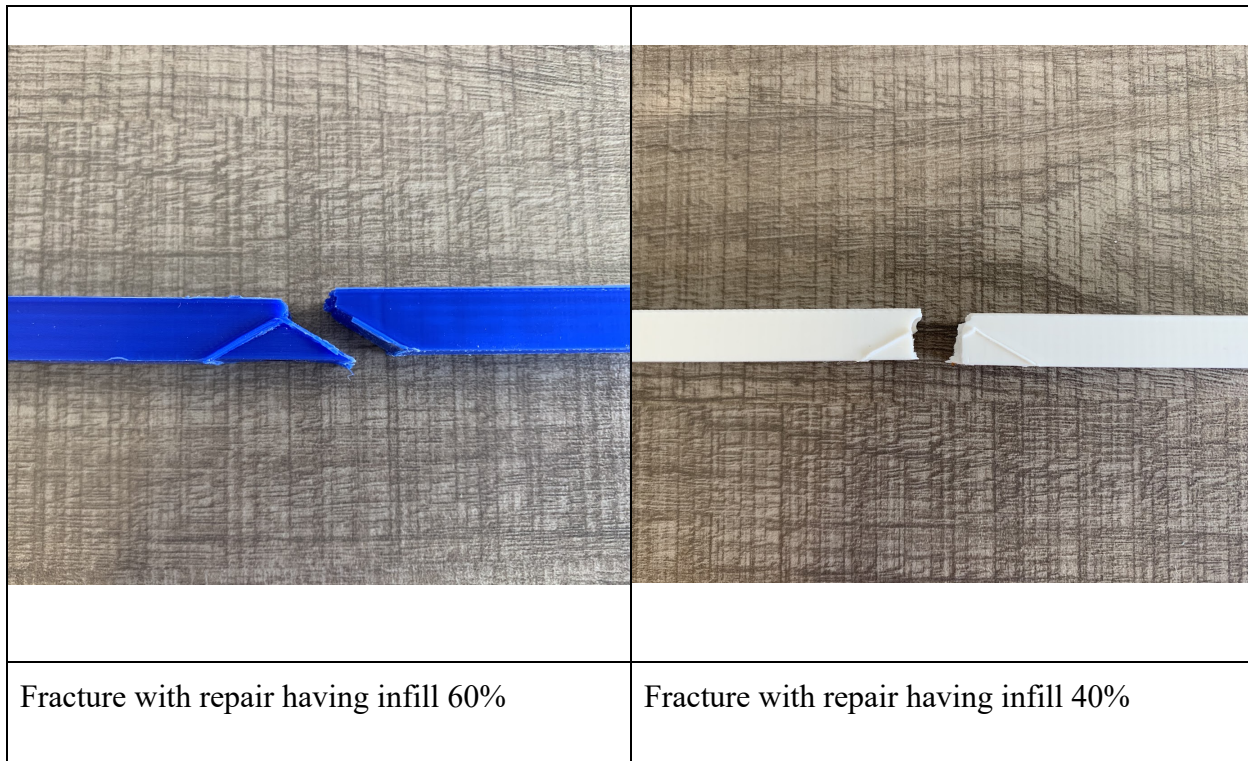


Figure X.

From our first testing of the T1 samples at different infills, we found the fracture to change as the infill of the repair changed. For 100-60% infill, the fracture is along the repair seam. This changes at 40% infill to break down the middle. For a max force F and length L the internal shear force is $F/2$ and internal moment is $FL/4$. For an infinitesimal element along the fracture at the bottom of the test piece (Figure Y, element 1) of the 100-60% infill, it would have the stresses shown in Figure Z.

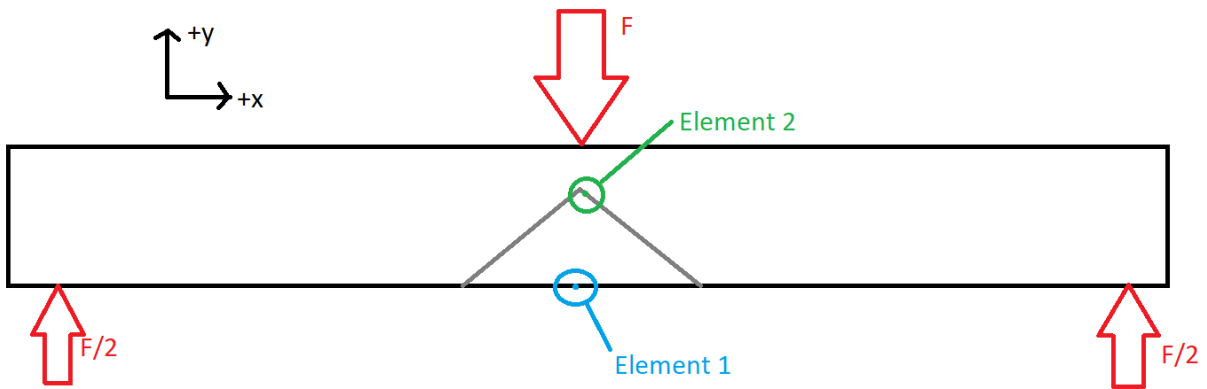


Figure Y. Location of elements on test piece

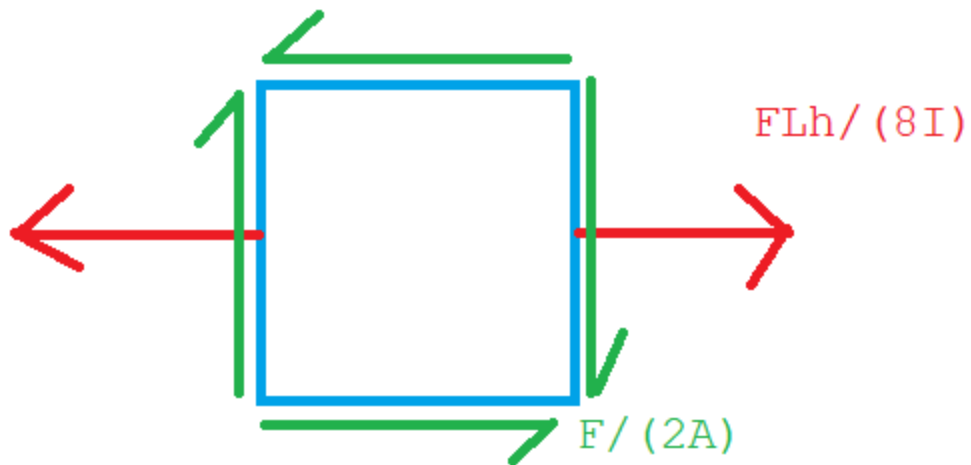


Figure Z. Element 1 Stresses

[Insert element 2 diagram](#)

Using the loading on these elements we can see that the interface between the damage and the repair can withstand a max shear strength of [], or max tensile strength of [].

Because of the layout of the repair, changing to orientation of the part during loading places different internal stresses on the repair. Loading the unrepaired side causes the entire part to bend downwards placing tension on the surface connection between the repair and damage. Placing the load on the repair causes the damaged part to compress on the repair at the surface connection. With potential damaged areas having the possibility of placing compression or tension loads on repairs, testing both the effects of different loading on our different tested repairs is necessary to find the best repair for a given scenario.

Find range for max shear strength of adhesion between damage and repair

4.5 Discussion/Conclusion

- Discuss outliers and possible causes
 - Repair adhesion failure?
 - Possible variability in adhesion

Chapter 5: Future Work

5.1 Adaptive In-Situ Printing (Tyler)

The application of this work has been operating under the assumption that the print location and its topography are known. This is to guarantee that the printer is aware of where exactly to deposit the material required for the repair. General print surfaces that require repair are not necessarily flat nor calibrated with the print head. Knowledge of the local conditions can be computed through a 3D scanning and point-cloud processing procedure. Light Detection and Ranging (LiDAR) is a burgeoning technology whose research advancements make it a natural contender for functioning as this scanner. In consideration for cost efficiency, triangulation scanners offer an inexpensive solution to scanning at shorter distances. This typically would be the case in reparative prints. For example, mounting a triangulation scanner to the manipulator adjacent to the print head would enable close-range scanning to the repair site. Ranging scans are not typically suitable for short-distance as the measurement error is often too large [16]. We would like to consider scanning methods that are on the order of centimeters. When paired with a capable robotic manipulator, this would enable a reasonable range in which both a scan and a print can be made.

The objective of this work in combination with scanning is general and adaptive reparative in-situ 3D printing. General voids or damages are not necessarily flat. In fact, a brief consideration for any type of damage on any type of mechanical structure would likely prompt a disorderly and irregular image. Mounting the print head onto a multiple degree-of-freedom (DOF) robotic manipulator is one way to provide a generic solution. Then, it would be possible

for the printer to deposit material in a sequence or in locations that common three-axis printers would not be able to achieve or reach. Using a six DOF manipulator, for example, would allow any print orientation within the robot's workspace. Utilizing more than six may ensure smooth printing due to the avoidance of kinematic singularities (where the solution for the robot's joints are discontinuous as the print head moves along a path).

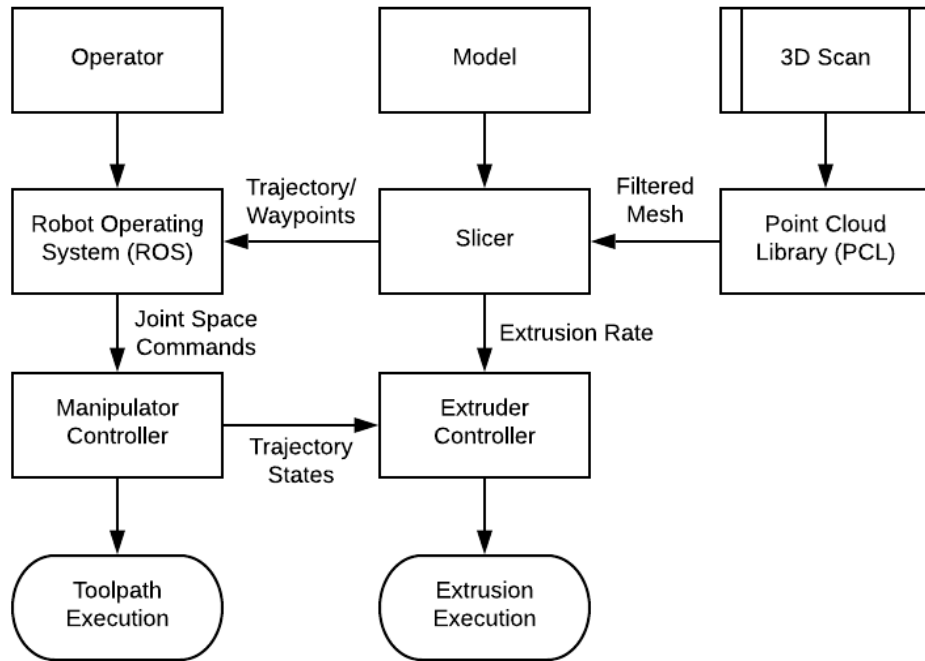


Figure X.Y Logical Flow of System Data

Figure X.Y represents a high-level design of how such a system would be implemented. Note that a 3D scan can be conducted offline. Scanning and printing do not have to occur sequentially. In the absence of a human expert to ensure that the point cloud produced is sensible, there is greater dependence on the scanning software and data processing reliability.

5.2 Materials

Sources are numbered in order corresponding to CH5 Source List document

Another area we wanted to study was composite filaments. Unfortunately, due to COVID, we had to readjust our goals midway through our project and decided that it was best to leave composite filaments for future work. Carbon Fiber PLA (CFPLA) is one of the most common reinforced filaments, and future researchers could conduct a very similar procedure to that described above to determine if CFPLA exhibits the similar patterns to PLA and ABS.

The print settings used for effective printing of CFPLA are very similar to that of PLA. The melting point still ranges from 200-230 degrees Celsius, and the bed adhesion will behave similarly to PLA [X]. However, the added fibers in the filament can cause clogging and increasing oozing while printing [X]. Experts recommend using a hardened steel nozzle to prevent damage to the extruder. To prevent clogs from starting to form in the tube, experts also suggest initially reducing the print speed by 25-50% [X]. These tradeoffs must be considered when deciding on a filament to test for our extruder.

CFPLA is a material steadily increasing in popularity due to its increased strength over PLA. There are two types of this material with the first being short fiber reinforced thermoplastics (SFRT) and the second being continuous fiber reinforced thermoplastics (CFRT) [26]. Short fiber reinforced thermoplastics consist of small pieces of carbon fiber embedded in the PLA filament. Continuous fiber reinforced thermoplastics consist of a long strand of carbon fiber embedded into the filament usually during the process of printing.

Future researchers could follow our testing procedures and document their results to compare the strengths vs PLA and ABS. It would be worthwhile to determine if either of these types, SFRT and CFRT, generates higher strengths than the other.

5.3 Extreme Environment

Sources are numbered in order corresponding to CH5 Source List document

An emerging field that may be able to make use of our research is the commercial space sector. In late 2021, NASA awarded contracts to Blue Origin, Northrop Grumman, and Nanoracks to build private space station in low Earth orbit (LEO) [17]. With private companies taking a stronghold on this new space race, there will be an increased risk in debris impacts with these large structures. Even with the most advanced debris tracking software at their disposal, sometimes small impacts happen. In May 2021, space debris hit the robotic arm on the International Space Station, leaving a hole in the arm [18]. These smaller objects cannot be tracked with current technology, so although the ISS is able to avoid large debris and satellites, there is always a risk for small collisions. These collisions have the potential to create damaged areas similar to the ones we investigated in our thesis. Below is a test from the European Space Agency of a simulated small debris impact at 15 kilometers per second [19].



Figure X. ESA Hypervelocity Impact Test. Credit ESA. [19]

Another rapidly increasing source of space debris that have the potential to generate collision events are anti-satellite missile tests. Although these are frowned upon by the scientific community and most space-faring nations, Russia and China have had a history of demonstrating their capability to destroy satellites in LEO. On November 15th 2021, Russia destroyed one of its old satellites with an anti-satellite missile [20]. According to the Arms Control Association, this single event created over 1500 trackable pieces of space debris that will stay in LEO for years to come [20]. Below is a graph of space debris vs time up until 2013, in which several vertical jumps are visible. These jumps represent large collision events, some of which are anti-satellite tests.

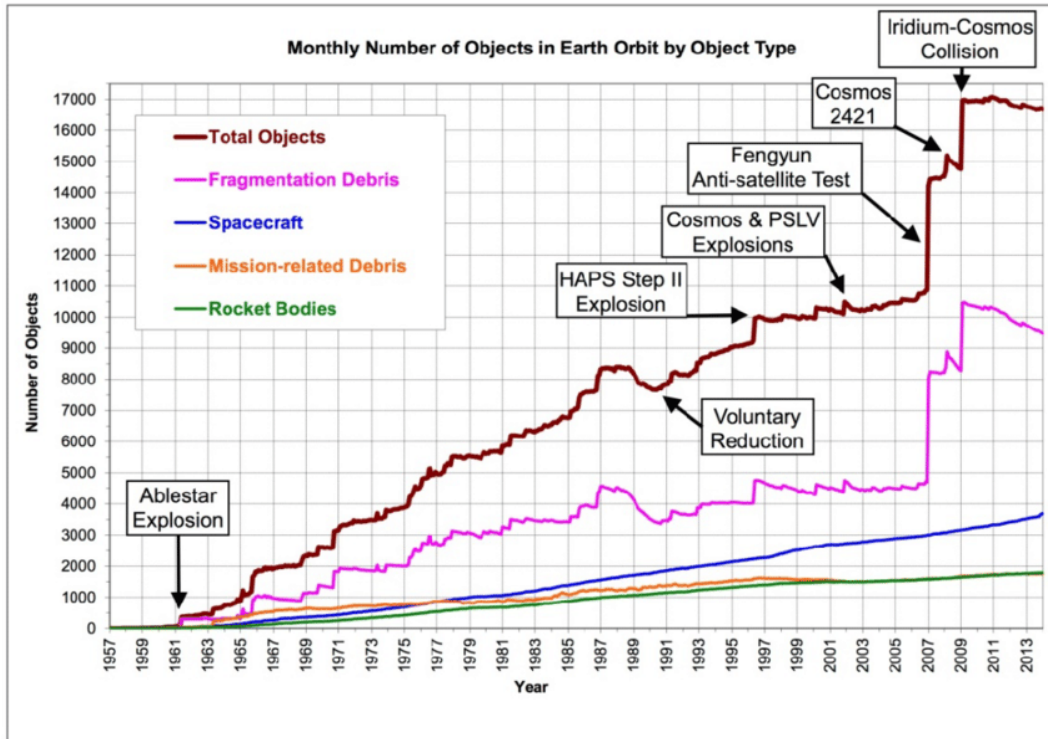


Figure X. Space Debris vs Time through 2014. Credit NASA. [5]

Satellite and space station collisions with debris are events that create situations similar to our research. Future researchers would need to investigate the effect of extreme temperatures on material properties and strength. A similar analysis could be conducted with SLM to determine the best repair method, and possibly the best repair time. For example, questions to ask could include: would it be better to print in extreme cold or extreme hot? how will these extreme temperature variations affect material properties during and after repair? if a repair is not possible in these conditions, would the printer need to create an artificial environment suitable for repair? Another area future researchers could dive into is the microgravity environment and printing. FDM partially relies on gravity to keep layers together as they cool. Other methods of 3D printing applicable to space stations and satellites may have similar challenges in space, which is something researchers would need to address.

Appendix

I. Timeline

II. Budget

III. Mentor Feedback

IV. Glossary

References